

## Particle-driven gravity currents down planar slopes

By ROGER T. BONNECAZE<sup>1</sup> AND JOHN R. LISTER<sup>2</sup>

<sup>1</sup>Department of Chemical Engineering, The University of Texas at Austin, Austin,  
TX 78712-1062, USA

<sup>2</sup>Institute of Theoretical Geophysics, Department of Applied Mathematics and  
Theoretical Physics, University of Cambridge, Silver St, Cambridge CB3 9EW, UK

(Received 17 July 1997 and in revised form 30 June 1998)

Particle-driven gravity currents, as exemplified by either turbidity currents in the ocean or ignimbrite flows in the atmosphere, are buoyancy-driven flows due to a suspension of dense particles in an ambient fluid. We present a theoretical study on the dynamics of and deposition from a turbulent current flowing down a uniform planar slope from a constant-flux point source of particle-laden fluid. The flow is modelled using the shallow-water equations, including the effects of bottom friction and entrainment of ambient fluid, coupled to an equation for the transport and settling of the particles. Two flow regimes are identified. Near the source and for mild slopes, the flow is dominated by a balance between buoyancy and bottom friction. Further downstream and for steeper slopes, entrainment also affects the behaviour of the current. Similarity solutions are also developed for the simple cases of homogeneous gravity currents with no settling of particles in the friction-dominated and entrainment-dominated regimes. Estimates of the width and length of the deposit from a monodisperse particle-driven gravity current with settling are derived from scaling analysis for each regime, and the contours of the depositional patterns are determined from numerical solution of the governing equations.

---

### 1. Introduction

Particle-driven gravity currents, or turbidity currents, are buoyancy-driven flows due to a suspension of dense particles. An understanding of these flows has applications to many geological, oceanographical and environmental processes. One important economic example is the emplacement of sediment that ultimately forms so-called turbiditic oil reservoirs (Wesser 1977; Perrodon 1985; Mutti 1992). Another rather spectacular and potentially dangerous example is the pyroclastic flow of hot gas and particles from a volcanic eruption (Simpson 1987).

Previously, we have studied theoretically and experimentally the behaviour of two-dimensional and axisymmetric particle-driven gravity currents flowing over horizontal surfaces due to either a fixed-volume release or a constant input of particle-laden fluid (Bonnetcaze, Huppert & Lister 1993, 1996; Bonnetcaze *et al.* 1995; Sparks *et al.* 1993). We developed a model based on the shallow-water equations for the conservation of mass and momentum of the fluid and a convective-transport equation for the conservation and settling of particles. The model was shown to describe successfully

the dynamics of and deposition from turbidity currents in the laboratory in a variety of situations. These include turbidity currents composed of polydisperse suspensions (Bonnecaze *et al.* 1996) and turbidity currents with reversing buoyancy due to the suspension of particles in an interstitial fluid that is less dense than the ambient (Sparks *et al.* 1993). Dade & Huppert (1994, 1995, 1996) have applied so-called box models of these flows to describe geological observations, such as the Black Shale turbidite off the coast of Cape Hatteras and the emplacement of an ignimbrite deposit from the Taupo volcano.

In all these studies the effects of entrainment of ambient fluid have been neglected. Ellison & Turner (1959) found that entrainment can significantly affect the dynamics of a homogeneous one-dimensional current flowing down a slope. They found that the rate of entrainment can be fitted empirically by the product of the local speed of the current and an entrainment coefficient  $E$ , which is a function of the slope, the velocity of the current and the density difference between the current and the ambient fluid (Ellison & Turner 1959; Turner 1973, pp. 178–186). These dependences can be captured by correlating  $E$  with the Richardson number, defined as the ratio of the buoyancy force to the inertial shear force. Recently, Hallworth *et al.* (1994, 1996) studied experimentally the entrainment in homogeneous currents created by the release of a fixed volume of dense saline fluid and flowing over a horizontal surface.

In this paper we study theoretically the behaviour of turbulent homogeneous and particle-driven gravity currents flowing down a planar slope from a constant source of dense fluid in a deep ambient fluid. Such a flow might occur, for example, at the outlet of a submarine canyon at the base of a continental shelf, which acts as a hydraulic control for a turbidity flow created by a submarine landslide at the top of the shelf and issuing from the canyon onto the abyssal slope. The outline of the paper is as follows. In §2 we modify the shallow-water equations to include the effects of entrainment and friction, which are important for turbulent gravity currents down slopes. These equations capture quite generally the effects of inertia, buoyancy and friction as well as entrainment. However, the equations are simplified by the identification of two flow regimes. We show in §3 that, for mild slopes and near the source, the flow is dominated by a force balance between friction and buoyancy; the effects of inertia and entrainment are negligible. For this regime we first develop a similarity solution for the case of a homogeneous gravity current (no settling of particles), including an analytic formula for the cross-slope extent of the flow. We then apply a scaling analysis to the governing equations for a turbidity current (with particle settling) in order to determine the characteristic dimensions of the flow and its deposit. With these we are able to write a dimensionless set of equations describing the flow which contain no dimensionless groups and are thus independent of all the physical parameters. These equations are solved once numerically to determine the universal deposition pattern for this system. In the second flow regime, which is discussed in §4 and applies for steeper slopes and further from the source, entrainment becomes important in addition to the effects of friction and buoyancy. A similarity solution is again derived for a homogeneous current, the equations scaled and, in a manner similar to that for the case of no entrainment, we determine the universal deposition pattern from turbidity currents in this regime. Finally, in §5 we conclude with a brief summary of the results and a means to determine which depositional regime is pertinent based on the inlet conditions and nature of the slope.

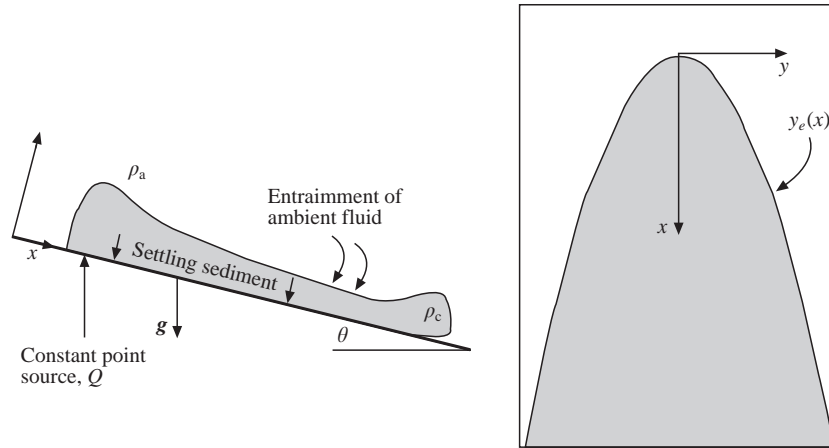


FIGURE 1. Profile and plan view of a gravity current due to a constant source of dense particle-laden fluid on a planar slope.

## 2. Model equations

Consider a particle-driven gravity current flowing from a constant source of fluid down a planar slope tilted at an angle  $\theta$  to the horizontal (figure 1). We assume that the flow rate is sufficiently large that the current is turbulent and that the turbulence keeps the particles vertically well-mixed over the current thickness  $h(x, y)$ , where  $x$  and  $y$  are the down-slope and cross-slope directions. The current has a bulk density  $\rho_c(x, y)$  and is flowing under a deep layer of ambient fluid of density  $\rho_a$ . The current is composed of monodisperse particles of density  $\rho_p$  suspended in the ambient fluid. The density of the gravity current is a volume average of the densities of the particles and the ambient interstitial fluid and hence is given by

$$\rho_c(\phi) = \rho_p \phi \phi_0 + \rho_a (1 - \phi \phi_0), \quad (2.1)$$

where  $\phi_0$  is the volume fraction of particles at the source and  $\phi(x, y)$  is the proportion of these still in suspension.

The thickness of the current  $h(x, y)$  varies slowly along the current, except perhaps in a small region very near the source. The mean down-slope and cross-slope velocities,  $u(x, y)$  and  $v(x, y)$ , predominate and there is only a very small vertical component of the flow. Here we take vertical to be perpendicular to the slope. The assumption of vertical uniformity of  $u$  and  $v$  parallels the assumption that the particles are vertically well-mixed. Thus, we may neglect vertical accelerations and assume a hydrostatic pressure gradient within the current, which only depends on the local density of the current  $\rho_c(\phi)$ , provided that  $h \tan \theta / x \ll 1$  (Mahrt 1982).

In addition to the buoyancy and inertial forces acting on the current, we also allow for entrainment of ambient fluid and bottom friction. We follow the model of Ellison & Turner (1959) which assumes that the rate of entrainment is the product of the local speed of the flow and an entrainment coefficient  $E$ . Frictional forces due to shear stresses on the bottom of the current are included in the momentum equation. We assume that the frictional drag is generated primarily by inertial effects, and so it varies quadratically with the velocity and with a constant of proportionality given by a friction coefficient  $c_f$ .

Under these conditions we may describe the current by modified two-dimensional

shallow-water equations, which for steady flow are given by

$$\nabla \cdot (\mathbf{u}h) = E|\mathbf{u}|, \quad (2.2)$$

$$\nabla \cdot (\mathbf{u}h\mathbf{u}) + \frac{1}{2}\nabla(g'_0 \cos \theta \phi h^2) - g'_0 \sin \theta \phi h \mathbf{e}_x = -\frac{1}{2}c_f |\mathbf{u}|\mathbf{u}, \quad (2.3)$$

where  $\mathbf{u} = (u, v)$  is the vector of the down-slope and cross-slope velocities,  $\mathbf{e}_x$  is the unit vector in the  $x$ -direction,  $\nabla$  is the two-dimensional gradient operator,  $g'_0 = (\rho_p - \rho_a)\phi_0 g / \rho_a$  is the initial reduced gravity and  $g$  is the gravitational acceleration. We have assumed that  $\phi_0 \ll 1$  and  $(\rho_p - \rho_a)\phi_0 / \rho_a \ll 1$ , and used the Boussinesq approximation, which includes the effects of  $\phi$  only in the buoyancy terms and neglects the contribution of the particles to the mass and momentum fluxes. Note that the terms on the right-hand sides of (2.2) and (2.3) are the source of fluid due to entrainment and the sink of momentum due to friction, respectively.

The hydrostatic pressure distribution and driving buoyancy force in the current depend on the local volume fraction of particles. The concentration of particles varies throughout the current due to advection, settling and entrainment of ambient fluid. Here we neglect particle entrainment from the base of the flow on the assumption that the velocities are insufficient to lift deposited sediment into the current. However, as stated earlier, we do assume that the flow is sufficiently vigorous for turbulent mixing to maintain a vertically uniform particle concentration in the current, including entrained fluid. Further, we assume that the particles leave the current only through the viscous sublayer at the base with a flux  $v_s \phi \phi_0 \cos \theta$  (Einstein 1968; Martin & Nokes 1988), where  $v_s$  denotes the settling velocity of an isolated particle, which is appropriate when the concentration of particles is small. Conservation of particles for a steady two-dimensional flow is then given by

$$\nabla \cdot (\mathbf{u}h\phi) = -v_s \phi \cos \theta. \quad (2.4)$$

Equations (2.2)–(2.4) describe the effects of inertia, buoyancy, friction, entrainment and particle settling on the dynamics of and deposition from steady turbulent particle-driven gravity currents down a planar slope. These equations have been used successfully to model two-dimensional and axisymmetric gravity currents flowing over horizontal surfaces with negligible entrainment and friction (Bonnecaze *et al.* 1993, 1995, 1996). As we shall see, two flow regimes exist in the present case, namely flow with and without entrainment, and considerable simplifications can then be made to the governing equations.

### 3. Negligible entrainment

As mentioned earlier, Ellison & Turner (1959) were able to correlate their experimentally determined entrainment coefficient  $E$  with the Richardson number,  $Ri = g'_0 h \cos \theta / |\mathbf{u}|^2$ . For  $Ri \ll 1$  the entrainment coefficient reaches a maximum of about 0.09, but decreases monotonically and very rapidly for  $Ri > 0.1$ ; the entrainment coefficient is only about 0.001 for  $Ri = 1$ . This observation is explained by the tendency of entrained parcels of less dense ambient fluid to be buoyantly expelled from a denser current. The greater the contrast in density between the current and the ambient fluid, the more rapidly ambient fluid is expelled before it is mixed into the current by turbulence, which thus inhibits entrainment due to shear. The Richardson number can be interpreted as the ratio of the interface-stabilizing buoyancy forces to the destabilizing shear forces. The Richardson number is generally of order unity near the source, so the entrainment is small. The cumulative effect of this small

entrainment cannot be neglected sufficiently far away from the source, but it may be neglected near the source in a region the length of which decreases with increasing slope. An estimate of this length is given later in §4.

Further, as is demonstrated *a posteriori*, the dynamics of the current are dominated by a balance between buoyancy and friction, and so the effects of inertia can be neglected. With these simplifications, equations (2.2)–(2.4) become

$$\nabla \cdot (\mathbf{u}h) = 0, \quad (3.1)$$

$$u = \left( \frac{2g'_0 S_\theta \phi h}{c_f} \right)^{1/2} \quad \text{and} \quad v = -\frac{g'_0 C_\theta}{c_f u} \frac{\partial}{\partial y} (\phi h^2), \quad (3.2)$$

$$\nabla \cdot (\mathbf{u}\phi h) = -v_s \phi \cos \theta, \quad (3.3)$$

where the equations for the velocities in (3.2) are due to the dominant down-slope and cross-slope balances between gravitational and frictional forces, and  $C_\theta = \cos \theta$  and  $S_\theta = \sin \theta$ . It has been assumed in (3.2) that  $|\mathbf{u}| \sim u$ , which will be true sufficiently far from the source. We first show an analytic solution to equations (3.1)–(3.3) for a current in which the settling velocity of the particles is negligible or, equivalently, for a homogeneous current, and then proceed to determine a numerical solution for the case with particle settling.

### 3.1. Flow of a homogeneous current with negligible entrainment

For a steady, homogeneous current flowing down a planar slope with no entrainment,  $\phi = 1$ , and the down-slope and cross-slope velocities are functions of  $h$  only, namely,

$$u = \left( \frac{2g'_0 S_\theta h}{c_f} \right)^{1/2}, \quad (3.4)$$

and

$$v = -\frac{C_\theta}{S_\theta} \left( \frac{2g'_0 S_\theta h}{c_f} \right)^{1/2} \frac{\partial h}{\partial y}. \quad (3.5)$$

The down-slope velocity is determined by a balance between the down-slope frictional forces, proportional to  $u^2$  and the gravitational forces due to the slope of the planar surface over which the current flows. The cross-slope velocity is set by a balance between the dominant cross-slope frictional forces, proportional to  $uv$ , and the buoyancy forces due to cross-slope variations in the height of the current. Inserting (3.4) and (3.5) into the equation of mass conservation yields the nonlinear partial differential equation for  $h$ ,

$$\frac{\partial h^{3/2}}{\partial x} = \frac{C_\theta}{S_\theta} \frac{\partial}{\partial y} \left( h^{3/2} \frac{\partial h}{\partial y} \right). \quad (3.6)$$

The boundary conditions for this equation are that  $h$  vanishes at the edges or cross-slope extent of the current  $y_e(x)$  (figure 1), which must be determined simultaneously with  $h(x, y)$  for this free-boundary-value problem. Since there is no entrainment of ambient fluid, the integrated flow across any cross-section is conserved, and so the cross-slope extent of the current,  $y_e(x)$ , is set by the constraint of conservation of mass at any down-slope position. That is,

$$2 \int_0^{y_e(x)} u h \, dy = Q, \quad (3.7)$$

where  $Q$  is the volumetric flow rate of the source.

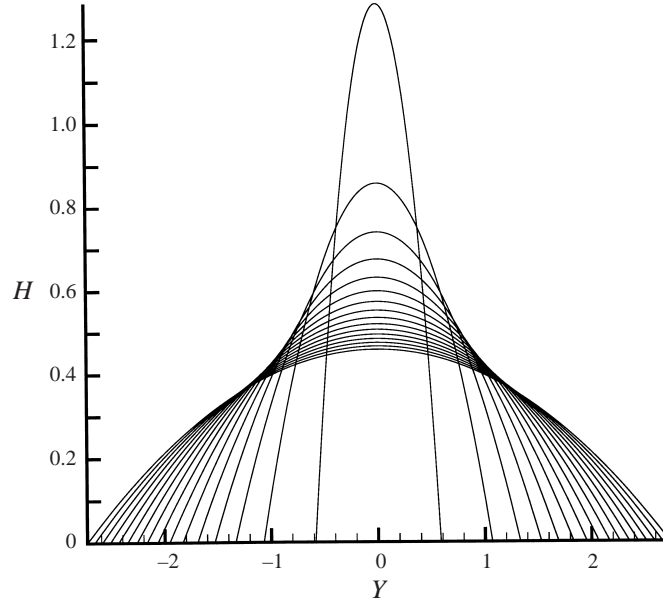


FIGURE 2. Similarity solution for the height  $H$  of a homogeneous gravity current with no entrainment as function of the cross-slope position  $Y$  for several values of the down-slope position  $X$ . The down-slope positions  $X$  range from 0.05 (inner profile) to 3.05 (outer profile) and are evenly spaced with intervals of 0.2.

Equations (3.4)–(3.7) can be solved analytically using a similarity transform for  $h$  given by (e.g. Lister 1990, p. 237)

$$h(x, y) = \eta_N^2 \left( \frac{c_f Q^2}{8g'_0 C_\theta} \right)^{1/4} x^{-1/4} G(\eta), \quad (3.8)$$

where

$$\eta = y/y_e(x), \quad (3.9)$$

$$y_e(x) = \eta_N \left( \frac{c_f Q^2 C_\theta^3}{8g'_0 S_\theta^4} \right)^{1/8} x^{3/8}, \quad (3.10)$$

$$G(\eta) = \frac{3}{16}(1 - \eta^2), \quad (3.11)$$

and

$$\eta_N = \left( \int_0^1 [G(\eta)]^{3/2} d\eta \right)^{-1/4} = \left( \frac{16}{3\pi^{2/5}} \right)^{5/8}. \quad (3.12)$$

Figure 2 illustrates the height of the current as a function of the down-slope and cross-slope positions. Note that in the figure  $h$ ,  $x$  and  $y$  have been non-dimensionalized by  $\hat{H}$ ,  $\hat{X}$ ,  $\hat{Y}$ , which are defined in the next subsection. The height of the current decreases down-slope as it spreads laterally. The height of the current is infinite at the origin since we have assumed a point source of fluid. To the best of our knowledge, this is the first analytic solution for turbulent flow down a planar slope due to a steady point source of fluid, and this solution complements the analogous solution for viscous flow given by Smith (1973).

Finally, given the similarity solution, the order of magnitude of the terms neglected in (2.3) decay at least  $O(x^{-1})$  faster than the dominant terms retained in (3.2). This justifies our assumption for sufficiently large  $x$ . We note for small  $x$  that the homogeneous gravity current is unaffected by the slope, and as can be shown, for example by following the method described by Lister (1992), it behaves like an axisymmetric flow from a point source flowing over a horizontal surface with a balance between inertial and buoyancy forces. The similarity solution describing this flow has been presented by Bonnecaze *et al.* (1995). By balancing the neglected inertial term of largest magnitude with those retained in equation (2.3), we find that the similarity solution described by equations (3.8)–(3.12) is valid for  $x \gg (Q^2/g'_0 C_\theta c_f^3)^{1/5}$ .

### 3.2. Turbidity current with negligible entrainment

As a turbidity current due to a constant flux of particle-laden fluid flows down the slope, it will deposit its particles over some characteristic down-slope and cross-slope length scales. These length scales, as well as characteristic dimensions for the height and velocities of the turbidity current, can be estimated using scaling arguments and the governing equations for the flow. The characteristic down-slope and cross-slope dimensions,  $\hat{X}$  and  $\hat{Y}$ , are proportional to the product of the characteristic down-slope and cross-slope velocities,  $\hat{U}$  and  $\hat{V}$ , and the characteristic time for settling,  $\hat{H}/v_s \cos \theta$ , where  $\hat{H}$  is the characteristic height of the current; that is,  $\hat{X} \sim \hat{U} \hat{H}/v_s \cos \theta$  and  $\hat{Y} \sim \hat{V} \hat{H}/v_s \cos \theta$ . From (3.4)–(3.5),  $\hat{U} \sim (2g'_0 S_\theta \hat{H}/c_f)^{1/2}$  and  $\hat{V} \sim (2g'_0 C_\theta^2 \hat{H}^3/c_f S_\theta \hat{Y}^2)^{1/2}$  and, since the flux down the slope is conserved,  $\hat{U} \hat{H} \hat{Y} \sim Q$ . Using these scalings yields

$$\hat{H} = \left( \frac{Q^4 v_s^2 c_f^3}{8g_0'^3 S_\theta} \right)^{1/11}, \quad (3.13)$$

$$\hat{X} = \left( \frac{2g_0' Q^6 S_\theta^4}{v_s^8 c_f C_\theta^{11}} \right)^{1/11}, \quad (3.14)$$

$$\hat{Y} = \left( \frac{Q^5 c_f}{2g_0' S_\theta^4 v_s^3} \right)^{1/11}, \quad (3.15)$$

from which  $\hat{U}$  and  $\hat{V}$  may be easily determined. For slowly settling particles  $\hat{X} \gg \hat{Y}$ .

Letting  $H = h/\hat{H}$ ,  $U = u/\hat{U}$ ,  $V = v/\hat{V}$ ,  $X = x/\hat{X}$  and  $Y = y/\hat{Y}$ , equations (3.1)–(3.3) can usefully be non-dimensionalized to yield

$$\frac{\partial UH}{\partial X} + \frac{\partial VH}{\partial Y} = 0, \quad (3.16)$$

$$U = (\phi H)^{1/2} \quad \text{and} \quad V = -\frac{1}{(\phi H)^{1/2}} \frac{\partial}{\partial Y} \left( \frac{1}{2} \phi H^2 \right), \quad (3.17)$$

$$\frac{\partial UH\phi}{\partial X} + \frac{\partial VH\phi}{\partial Y} = -\phi. \quad (3.18)$$

Clearly, these non-dimensionalized equations are independent of all the physical parameters in the problem. Hence, they are universal equations that describe the dynamics of and deposition from a turbidity current flowing down a planar slope with negligible entrainment. The resulting universal deposition pattern can then be determined by solving (3.16)–(3.18) once, which must be done numerically. We have done so using an explicit central finite-difference method to yield the results illustrated in figures 3–5.

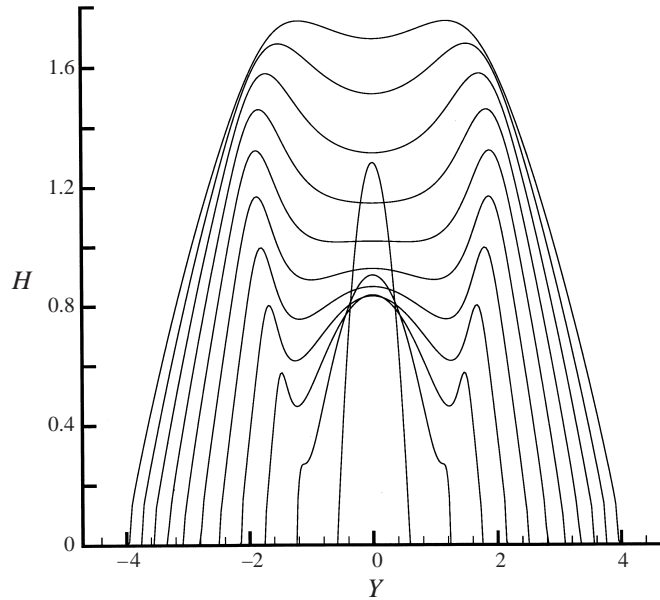


FIGURE 3. Numerical solution for the height  $H$  of a particle-driven gravity current with no entrainment as function of the cross-slope position  $Y$  for several values of the down-slope position  $X$ . The down-slope positions  $X$  range from 0.05 (inner profile) to 2.05 (outer profile) and are evenly spaced with intervals of 0.2.

Figure 3 shows the height of the turbidity current as a function of the down-slope and cross-slope positions. Initially, before too much sediment has been deposited, the height of the current behaves much like that of a homogeneous current. As a result, the rate of sedimentation is initially very much larger at the edges of the current since the height of the current is smaller in that region and so there is a relatively shorter average distance for the particles to settle. Thus, the volume fraction is less at the edges of the current (figure 4). With this relative loss of buoyancy compared to the interior of the flow, the cross-slope velocity near the edge of the current is not as large as that in the interior. So, as seen in figure 3, further from the source there is a relative accumulation of fluid near the edge since it can no longer expand as fast as a homogeneous current.

Since the interstitial fluid has been made just slightly more dense (0.01%) than the ambient fluid in order to simplify the numerical solution, the height of the current far down-slope ( $X \gg 1$ ) begins to approach again the quadratic shape of the self-similar homogeneous current. We confirmed that the dynamics of and deposition from the current were not appreciably different in the region of deposition by trying various values of the interstitial fluid density ranging from 0.001% to 0.05% greater than the ambient.

Figures 4 and 5 show two views of the volume fraction as a function of down-slope and cross-slope position. Figure 4 shows that the dominant path for sediment transport is along the centre or core of the flow since sedimentation is more rapid at the edges. Since the settling flux is proportional to  $\phi$ , the contours of the volume fraction of particles in the current in figure 5 can also be interpreted as the depositional pattern for a current flowing for some sufficiently long time that the steady-state behaviour of the flow dominates the build-up of the deposit. The contours can then be considered to be scaled by the density or depth of deposit at the origin. If there has



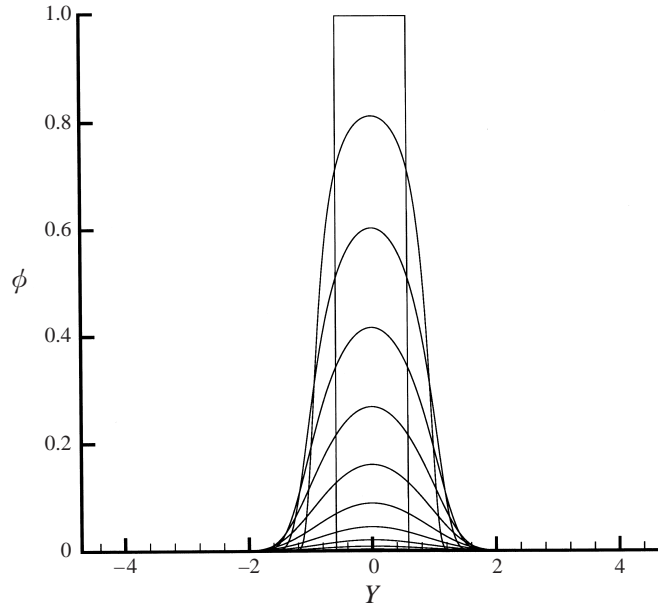


FIGURE 4. Numerical solution for the volume fraction of particles in a particle-driven gravity current with no entrainment as function of the cross-slope position  $Y$  for several values of the down-slope position  $X$ . The down-slope positions  $X$  range from 0.05 (inner profile) to 2.05 (outer profile) and are evenly spaced with intervals of 0.2.

been a steady flow for a period of time  $\Delta t$ , the density of deposit at the origin would be  $\rho_p v_s \phi_0 \cos \theta \Delta t$ . The deposit is clearly lobe-shaped and the dimensional down-slope and cross-slope extent of the deposits are obtained by rescaling with  $\hat{X}$  and  $\hat{Y}$ , where  $\hat{X} \gg \hat{Y}$ . Assuming that the extent of the deposit is defined by the contour  $\phi = 0.01$ , the down-slope and cross-slope extent of the deposit are approximately  $1.8\hat{X}$  and  $3.2\hat{Y}$ .

#### 4. Entrainment

In the previous section we neglected the effect of entrainment of ambient fluid on the dynamics and deposition associated with homogeneous or turbid gravity currents. The justification for this assumption rests on the small value of the entrainment coefficient ( $E \ll 0.1$ ), which applies particularly for mild slopes. While some entrainment is of course occurring, the fraction of entrained ambient fluid can be shown to be negligible in comparison to the original interstitial fluid of the current. Further from the source, however, entrainment becomes significant as more of the current is composed of entrained ambient fluid. This can be seen by comparing the magnitudes of the terms in (2.2) using the results from the similarity solution (3.8) for the homogeneous current with no entrainment. The left-hand side of (2.2) is  $O[(g'_0 S_\theta / c_f)^{1/2} (c_f Q^2 / g'_0 C_\theta)^{3/8} x^{-11/8}]$ . The magnitude of the right-hand side is  $O[E (g'_0 S_\theta / c_f)^{1/2} (c_f Q^2 / g'_0 C_\theta)^{1/8} x^{-1/8}]$ . For small entrainment coefficients  $E$ , we may thus neglect the right-hand side, but the assumption is not uniformly valid; at a transition distance  $x_t \sim (c_f Q^2 / g'_0 C_\theta E^4)^{1/5}$  the effects of entrainment become as important as the flow of the original fluid. However, even accounting for entrainment, equations (2.2)–(2.4) can be simplified as follows.

Following a procedure similar to that of §3.2, we determine the characteristic

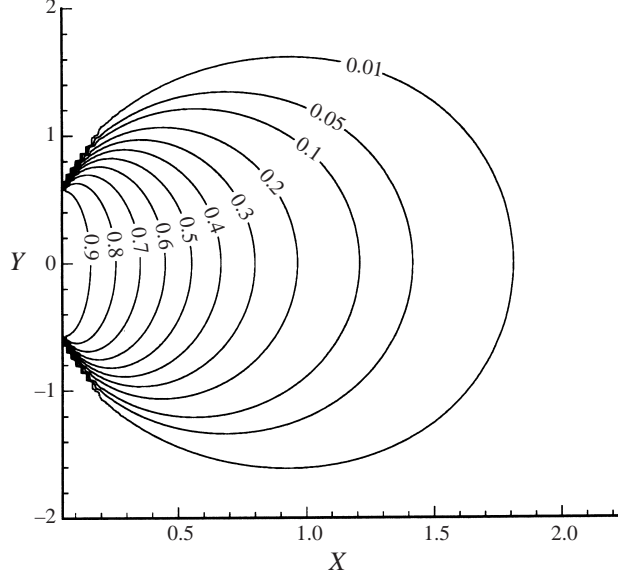


FIGURE 5. Contours of the normalized depth or density of deposit from a particle-driven gravity current with no entrainment as function of down-slope and cross-slope positions. The coordinates are non-dimensionalized by  $\hat{X}$  and  $\hat{Y}$ .

down-slope and cross-slope velocities and the lengths and thickness of a turbid entraining current. We non-dimensionalize (2.2)–(2.4) by letting  $\mathcal{U} = u/\tilde{U}$ ,  $\mathcal{V} = v/\tilde{V}$ ,  $\mathcal{H} = h/\tilde{H}$ ,  $\mathcal{X} = x/\tilde{X}$  and  $\mathcal{Y} = y/\tilde{Y}$ , where  $\tilde{U} = v_s C_\theta/E$ ,  $\tilde{V} = (C_\theta^3/ES_\theta)^{1/2}v_s$ ,  $\tilde{X} = (4g_0'^2 Q^2 E^5 S_\theta^3/C_\theta^7 c_f v_s^6)^{1/2}$ ,  $\tilde{H} = E\tilde{X}$  and  $\tilde{Y} = (EC_\theta/S_\theta)^{1/2}\tilde{X}$ . The volume fraction is also rescaled so that  $\Phi = \phi/\tilde{\Phi}$ , where  $\tilde{\Phi} = (c_f v_s^2 C_\theta^2/2g_0' S_\theta E^3 \tilde{X})$ . The resulting dimensionless equations are then given by

$$\frac{\partial \mathcal{U} \mathcal{H}}{\partial \mathcal{X}} + \frac{\partial \mathcal{V} \mathcal{H}}{\partial \mathcal{Y}} = (\mathcal{U}^2 + E\mathcal{V}^2/T_\theta)^{1/2}, \quad (4.1)$$

$$\frac{2E}{c_f} \left[ \frac{\partial}{\partial \mathcal{X}} (\mathcal{U}^2 \mathcal{H}) + \frac{\partial}{\partial \mathcal{Y}} (\mathcal{U} \mathcal{V} \mathcal{H}) \right] + \frac{E}{2T_\theta} \frac{\partial}{\partial \mathcal{X}} (\Phi \mathcal{H}^2) - \Phi \mathcal{H} = -(\mathcal{U}^2 + E\mathcal{V}^2/T_\theta)^{1/2} \mathcal{U}, \quad (4.2)$$

$$\frac{2E}{c_f} \left[ \frac{\partial}{\partial \mathcal{X}} (\mathcal{U} \mathcal{V} \mathcal{H}) + \frac{\partial}{\partial \mathcal{Y}} (\mathcal{V}^2 \mathcal{H}) \right] + \frac{\partial}{\partial \mathcal{Y}} (\frac{1}{2} \Phi \mathcal{H}^2) = -(\mathcal{U}^2 + E\mathcal{V}^2/T_\theta)^{1/2} \mathcal{V}, \quad (4.3)$$

$$\frac{\partial \mathcal{U} \mathcal{H} \Phi}{\partial \mathcal{X}} + \frac{\partial \mathcal{V} \mathcal{H} \Phi}{\partial \mathcal{Y}} = -\Phi, \quad (4.4)$$

where  $T_\theta = \tan \theta$ .

The equations may be simplified as follows. Typical friction factors  $c_f$  for a seabed, which may be estimated by using Manning's equation and the associated roughness coefficients for open channel flow (e.g. Whitaker 1984, pp. 350–353), are of order 0.005 to 0.02. On examination of the data for entrainment taken by Ellison & Turner (1959), we find that  $E \approx 10^{-3}$  for  $Ri \approx 1$ . For a Richardson number of  $O(1)$ , we may then assume that  $2E/c_f \ll 1$ . Thus, (4.1)–(4.4) simplify to become

$$\frac{\partial \mathcal{U} \mathcal{H}}{\partial \mathcal{X}} + \frac{\partial \mathcal{V} \mathcal{H}}{\partial \mathcal{Y}} = \mathcal{U}, \quad (4.5)$$

$$\mathcal{U} = (\Phi \mathcal{H})^{1/2} \quad \text{and} \quad \mathcal{V} = -\frac{1}{(\Phi \mathcal{H})^{1/2}} \frac{\partial}{\partial \mathcal{Y}} \left( \frac{1}{2} \Phi \mathcal{H}^2 \right), \quad (4.6)$$

$$\frac{\partial \mathcal{U} \mathcal{H} \Phi}{\partial \mathcal{X}} + \frac{\partial \mathcal{V} \mathcal{H} \Phi}{\partial \mathcal{Y}} = -\Phi. \quad (4.7)$$

As in the case of no entrainment, the down-slope and cross-slope velocities are determined by a local balance between buoyancy and frictional forces. The dominant contribution to entrainment is due, not surprisingly, to the larger down-slope velocity. Dimensionally, the down-slope velocity of the fluid is  $u = (2g'_0 h \sin \theta / c_f)^{1/2}$ , and the Richardson number  $Ri = c_f / 2 \tan \theta$ . Thus, for  $Ri = O(1)$  and for equations (4.5)–(4.7) to be valid requires  $\tan \theta \ll c_f$ .

Before solving the equations for a turbidity current, it is instructive first to solve the equations for the case of a homogeneous current as described in the next subsection.

#### 4.1. Homogeneous current with entrainment

Equations (4.5)–(4.7), rewritten in dimensional form, are

$$\frac{\partial uh}{\partial x} + \frac{\partial vh}{\partial y} = Eu, \quad (4.8)$$

$$u = \left( \frac{2g'_0 S_\theta \phi h}{c_f} \right)^{1/2} \quad \text{and} \quad v = -\frac{g'_0 C_\theta}{c_f u} \frac{\partial}{\partial y} (\phi h^2), \quad (4.9)$$

$$\frac{\partial uh\phi}{\partial x} + \frac{\partial vh\phi}{\partial y} = 0. \quad (4.10)$$

Although here no particles are lost by settling, the concentration of the dense component driving the flow is reduced due to entrainment of the ambient fluid. Hence, the conservation of buoyancy expressed in (4.10) must be retained unlike the case for a homogeneous current with no entrainment. Since there is no settling, the total buoyancy flux at any cross-section must be conserved so that

$$2 \int_0^\infty uh\phi \, dy = Q, \quad (4.11)$$

where here the current is shown below to have infinite cross-slope extent at steady-state due to entrainment. There is a similarity solution to (4.8)–(4.10) in which

$$h(x, y) = \frac{3}{5} Ex, \quad (4.12)$$

$$\phi(x, y) = \frac{5}{3} \left( \frac{5Q^2 c_f}{6\pi g'_0 E^4 C_\theta} \right)^{1/3} x^{-5/3} e^{-\eta^2}, \quad (4.13)$$

and

$$\eta = \left( \frac{5S_\theta}{3EC_\theta} \right)^{1/2} \frac{y}{x}. \quad (4.14)$$

Figure 6 shows the dimensionless product  $\Phi \mathcal{H}$ , which is proportional to the buoyancy force in the flow, across the current for several locations down-slope based on the above solution. It is clear that most of the particles are confined to the central region of the flow. This is because the velocities needed to advectively transport the particles depend on the presence of particles to create the buoyancy force needed to drive them. Although the form of the solution for the height of the current implies that the current is of infinite extent in the cross-slope direction, the fact that the

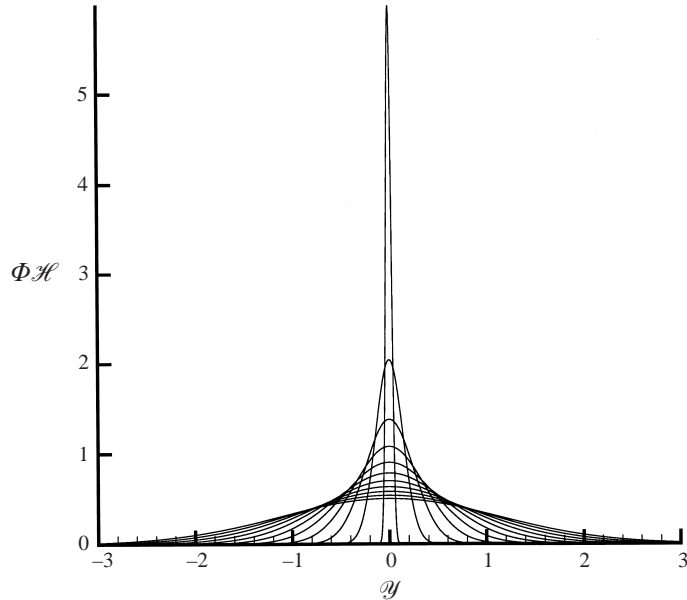


FIGURE 6. The buoyancy  $\Phi\mathcal{H}$  as a function of  $\mathcal{Y}$  in a particle-driven gravity current with entrainment but no settling. The several profiles are for varying  $\mathcal{X}$  ranging from 1.2 (inner profile) to 6.2 (outer profile) and are evenly spaced with intervals of 0.5.

volume fraction of particles and  $\Phi\mathcal{H}$  decay exponentially away from the centre of the flow means that the practical extent of the current is finite. Taking the locus of points where the volume fraction of the particles is one percent of the value along the centreline, the approximate cross-slope extent of the current is given by

$$y_e(x) \approx 1.66 \left( \frac{EC_\theta}{S_\theta} \right)^{1/2} x, \quad (4.15)$$

showing that it grows linearly with down-slope distance.

#### 4.2. Turbidity current with entrainment

Unfortunately, there is no analytic solution to (4.5)–(4.7) which describe the dynamics and deposition of a turbidity current down a planar slope with entrainment. However, as was noted earlier, these are universal equations independent of all the dimensional parameters. They may thus be solved once numerically to determine a master curve for the deposition of particles. Again, we used an explicit central finite-difference method to yield the results illustrated in figures 7–9. The initial conditions in  $\mathcal{X} \ll 1$  were those of a homogeneous current with entrainment, with the height and volume fraction of particles set to zero at large values of  $|\mathcal{Y}|$  for numerical convenience. The location of the truncation of the current had no effect on the deposition patterns if it were located at two or more times the extent of a homogeneous current estimated in (4.15).

Figure 7 depicts the volume fraction of particles as a function of  $\mathcal{Y}$  for several locations down-slope. It is also clear in this regime that the majority of the flow is confined to a central core in the current. Figure 8 depicts the height of the current near to and far from the source. Along the central core of the current, we observe that the height of the current increases linearly with the distance down-slope as expected

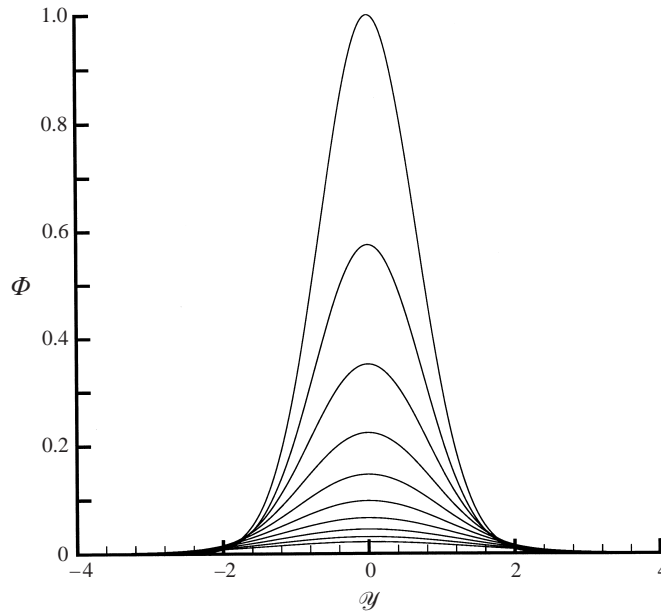


FIGURE 7. The volume fraction of particles  $\Phi$  in a particle-driven gravity current with entrainment and settling as a function of cross-slope position  $y$ . The profiles are for varying  $X$  ranging from 1.2 (highest profile) to 3.0 (lowest profile) and are evenly spaced with intervals of 0.2.

for a homogeneous current. Note that at large distances down-slope the height of the current again begins to flatten like that of a homogeneous current. This is because for numerical convenience the interstitial fluid of the current was made slightly denser than that of the ambient and so after the particles have settled it behaves like a homogeneous current. Figure 9 illustrates the contours of the density of deposit for a current flowing for a sufficiently long-time that the steady-state behaviour of the flow dominates its nature. The contours are scaled by the deposit at the origin for some specific time. The deposit is lobe-shaped and the dimensional down-slope and cross-slope extents are scaled by  $\tilde{X}$  and  $\tilde{Y}$ . Assuming that the extent of the deposit is defined by the contour  $\Phi = 0.01$ , the down-slope and cross-slope extent of the deposit are approximately  $3.4\tilde{X}$  and  $4.5\tilde{Y}$ .

## 5. Conclusions

We have theoretically described the steady-state behaviour of turbulent homogeneous and particle-driven gravity currents flowing down a planar slope due to a steady, point source of dense fluid both with and without entrainment of the ambient fluid. Near the source and for mild slopes, it was found that the dynamics were dominated by a balance between the buoyancy and frictional forces, and far from the source and for steeper slopes, entrainment also becomes significant. For the homogeneous currents similarity solutions were determined that describe the height and buoyancy distribution in the flows and determine the extent of the currents,  $y_e(x)$ . In particular it was found that for down-slope positions  $x \gtrsim (Q^2/g'_0 C_\theta c_f^3)^{1/5}$ , when the current no longer behaves as an axisymmetric current on a horizontal surface and the effect of the slope is important, the cross-slope extent of a current initially varies like  $y_e(x) \sim x^{3/8}$  without entrainment. When the down-slope position

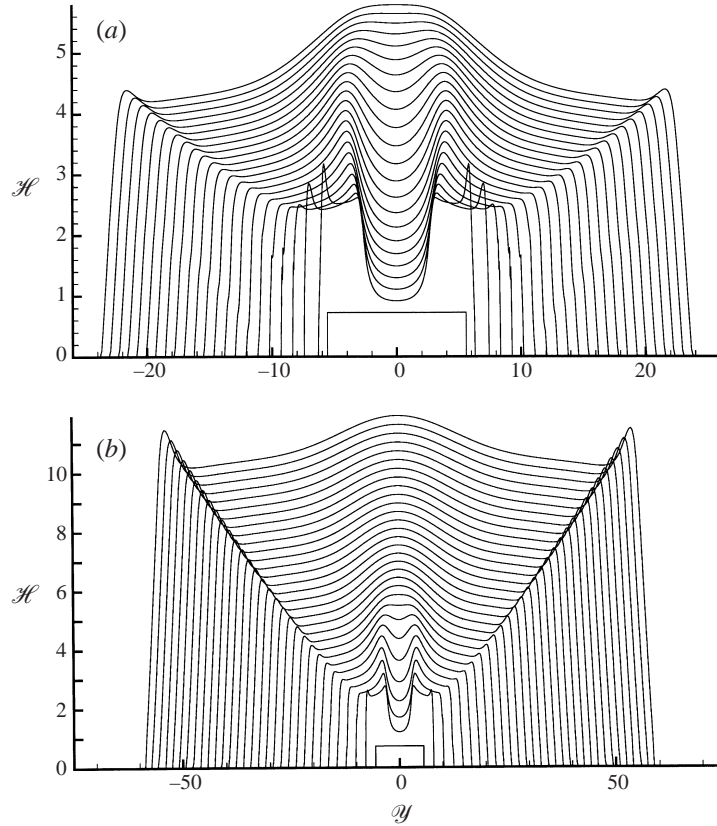


FIGURE 8. The height  $\mathcal{H}$  of a particle-driven gravity current with entrainment and settling as a function of the cross-slope position  $y$  for a smaller (a) and larger (b) range of  $\mathcal{X}$ . The profiles are for varying  $\mathcal{X}$  ranging from (a) 1.2 (lowest profile) to 5.6 (highest profile), evenly spaced with intervals of 0.2, and (b) 1.2 (lowest profile) to 16.2 (highest profile), evenly spaced with intervals of 0.5.

	Down-slope extent	Cross-slope extent
No entrainment	$1.8 \left( \frac{2g'_0 Q^6 S_\theta^4}{v_s^8 c_f C_\theta^{11}} \right)^{1/11}$	$3.2 \left( \frac{Q^5 c_f}{2g'_0 S_\theta^4 v_s^3} \right)^{1/11}$
Entrainment	$3.4 \left( \frac{4g'^2 Q^2 E^5 S_\theta^3}{C_\theta^6 c_f^2 v_s^6} \right)^{1/2}$	$4.5 \left( \frac{2g'_0 Q E^3 S_\theta}{C_\theta^3 c_f v_s^3} \right)$

TABLE 1. Down-slope and cross-slope extent of the deposit from a turbidity current defined as the distance where the depth or density of deposit is 1% of the maximum value at the origin.

$x \gtrsim (c_f Q^2 / g'_0 C_\theta E^4)^{1/5}$ , the cumulative effects of entrainment become important and  $y_e(x) \sim x$ .

In the case of particle-driven or turbidity currents, both with and without entrainment, a scaling analysis of the governing equations produced characteristic dimensions, in particular the down-slope and cross-slope extents of the deposit. Using these characteristic dimensions, the equations were rescaled to produce sets of equations

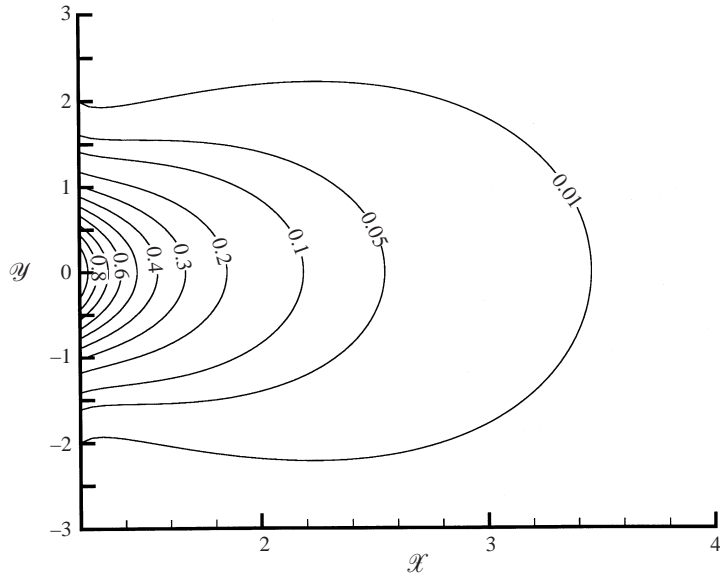


FIGURE 9. Contours of the normalized depth or density of deposit from a particle-driven gravity current with entrainment as function of down-slope and cross-slope positions. The coordinates are non-dimensionalized by  $\hat{X}$  and  $\hat{Y}$ .

independent of any of the dimensional parameters. These were solved numerically to determine the universal deposition patterns from turbidity flows with and without entrainment. Table 1 summarizes the extent of these deposits in terms of the characteristic dimensions. We may estimate whether deposition occurs predominantly in the entraining or non-entraining regime using  $x_t$  for a homogeneous current. For  $x_t \ll \hat{X}$  deposition will occur in the regime of non-entrainment, but for  $x_t \gg \hat{X}$ , deposition will occur in the entraining regime. Finally, we note that extent of deposit created by certain unsteady inflows of particle-laden fluid may be determined by scaling analyses similar to those presented here. An example is shown in the Appendix.

R.T.B. gratefully acknowledges NERC for supporting a summer visit to Cambridge where this work was begun and the intellectually stimulating environment and hospitality provided by Professor H. E. Huppert, the ITG and DAMTP.

#### Appendix. Extent of deposit for volumetric inputs of $Qt^\alpha$

Scaling arguments similar to those given in §3.2 and §4 for non-entraining and entraining turbidity currents due to a constant flux of particle-laden fluid may be used to estimate the down-slope and cross-slope extent of deposits for turbidity currents with a volumetric input equal to  $Qt^\alpha$ , where  $\alpha$  is a non-negative constant. The case of a constant flux input is  $\alpha = 1$ . We note that, following techniques illustrated in Lister (1992), one may also determine the down-slope and cross-slope extents of homogeneous currents with unsteady inputs, and in fact show that the near-source behaviour of the currents is that due to a steady flow with an instantaneous flux of strength  $\alpha Qt^{\alpha-1}$ . However, our interest here is with the behaviour of particle-laden flows.

For a turbidity current with negligible entrainment, the characteristic down-slope and cross-slope dimensions,  $\hat{X}$  and  $\hat{Y}$ , are proportional to the product of the char-

acteristic down-slope and cross-slope velocities,  $\hat{U}$  and  $\hat{V}$ , and the characteristic time for settling,  $\hat{H}/v_s \cos \theta$ , where  $\hat{H}$  is the characteristic height of the current; that is,  $\hat{X} \sim \hat{U}\hat{H}/v_s \cos \theta$  and  $\hat{Y} \sim \hat{V}\hat{H}/v_s \cos \theta$ . From (3.4)–(3.5),  $\hat{U} \sim (2g'_0 S_\theta \hat{H}/c_f)^{1/2}$  and  $\hat{V} \sim (2g'_0 C_\theta^2 \hat{H}^3/c_f S_\theta \hat{Y}^2)^{1/2}$  and, since the total input of particles must be conserved,  $\hat{H}\hat{X}\hat{Y} \sim Qt^\alpha$ . These scalings yield

$$\hat{X} = \left[ \left( \frac{2g'_0 Q^6 S_\theta^4}{v_s^8 c_f C_\theta^{11}} \right) \left( \frac{2g'_0 S_\theta v_s C_\theta}{c_f} \right)^{2(1-\alpha)} \right]^{1/(15-4\alpha)}, \quad (\text{A } 1)$$

$$\hat{Y} = \left[ \left( \frac{Q^5 c_f}{2g'_0 S_\theta^4 v_s^3} \right) \left( \frac{2g'_0 C_\theta^4 v_s^3}{c_f} \right)^{(1-\alpha)} \right]^{1/(15-4\alpha)}. \quad (\text{A } 2)$$

Note that for  $\alpha \geq 15/4$  no deposit of finite extent exists. For these cases, the extent of the deposit increases with time according to the extent of a homogeneous current because the height of the current increases with time at such a rate that particles, which are assumed vertically well-mixed, settle out more slowly than they are advected downstream.

For a turbidity current which entrains ambient fluid, the volume fraction must also be rescaled as was done in §4. As before, the characteristic down-slope and cross-slope dimensions,  $\tilde{X}$  and  $\tilde{Y}$ , satisfy  $\tilde{X} \sim \tilde{U}\tilde{H}/v_s \cos \theta$  and  $\tilde{Y} \sim \tilde{V}\tilde{H}/v_s \cos \theta$ . From (3.4)–(3.5), but including the dilution of  $\phi$  to a scale  $\tilde{\phi}$ ,  $\tilde{U} \sim (2g'_0 S_\theta \tilde{\phi} \tilde{H}/c_f)^{1/2}$  and  $\tilde{V} \sim (2g'_0 C_\theta^2 \tilde{\phi} \tilde{H}^3/c_f S_\theta \tilde{Y}^2)^{1/2}$  and, since the total input of particles must be conserved,  $\tilde{\phi}\tilde{H}\tilde{X}\tilde{Y} \sim Qt^\alpha$ . These scalings yield

$$\tilde{X} \sim \left[ \left( \frac{4g_0'^2 Q^2 E^5 S_\theta^3}{C_\theta^7 c_f^2 v_s^6} \right)^{1/2} \left( \frac{E}{v_s C_\theta} \right)^{(\alpha-1)} \right]^{1/(2-\alpha)}, \quad (\text{A } 3)$$

$$\tilde{Y} \sim \left[ \left( \frac{2g'_0 Q E^3 S_\theta}{c_f v_s^3 C_\theta^3} \right) \left( \frac{E \tilde{X}}{v_s C_\theta} \right)^{(\alpha-1)} \right]^{1/(2-\alpha)}. \quad (\text{A } 4)$$

For an entraining turbidity current, the deposit is finite only for  $\alpha < 2$ . For greater values of  $\alpha$  the deposit increases in extent as the rate of influx of particle-laden fluid increases according to that of a homogeneous current.

#### REFERENCES

- BONNETCAZE, R. T., HALLWORTH, M. A., HUPPERT, H. E. & LISTER, J. R. 1995 Axisymmetric particle-driven gravity currents. *J. Fluid Mech.* **294**, 93–121.
- BONNETCAZE, R. T., HUPPERT, H. E. & LISTER, J. R. 1993 Particle-driven gravity currents. *J. Fluid Mech.* **250**, 339–369.
- BONNETCAZE, R. T., HUPPERT, H. E. & LISTER, J. R. 1996 Patterns of sedimentation from polydispersed turbidity currents. *Proc. R. Soc. Lond. A* **452**, 2247–2261.
- DADE, W. B. & HUPPERT, H. E. 1994 Predicting the geometry of channelized deep-sea turbidites. *Geology* **22**, 645–648.
- DADE, W. B. & HUPPERT, H. E. 1995 Run-out and fine-sediment deposits of axisymmetric gravity currents. *J. Geophys. Res.* **100**, 18597–18609.
- DADE, W. B. & HUPPERT, H. E. 1996 Emplacement of the Taupo ignimbrite by a dilute turbulent flow. *Nature* **381**, 476–477.
- EINSTEIN, H. A. 1968 Deposition of suspended particles in a gravel bed. *J. Hydraul. Div. ASCE* **94**, 1197–1205.
- ELLISON, T. H. & TURNER, J. S. 1959 Turbulent entrainment in stratified flows. *J. Fluid Mech.* **6**, 423–448.



- HALLWORTH, M. A., HUPPERT, H. E., PHILLIPS, J. C. & SPARKS, R. S. J. 1996 Entrainment into two-dimensional and axisymmetric turbulent gravity currents. *J. Fluid Mech.* **308**, 289–311.
- HALLWORTH, M. A., PHILLIPS, J. C., HUPPERT, H. E. & SPARKS, R. S. J. 1994 Entrainment in turbulent gravity currents. *Nature* **362**, 829–831.
- LISTER, J. R. 1990 Buoyancy-driven fluid fracture: similarity solutions for the horizontal and vertical propagation of fluid-filled cracks. *J. Fluid Mech.* **217**, 213–239.
- LISTER, J. R. 1992 Viscous flows down an inclined plane from point and line sources. *J. Fluid Mech.* **242**, 631–653.
- MAHRT, L. 1982 Momentum balance of gravity flows. *J. Atmos. Sci.* **39**, 2701–2711.
- MARTIN, D. & NOKES, R. 1988 Crystal settling in a vigorously convecting magma chamber. *Nature* **332**, 534–536.
- MUTTI, E. 1992 Turbidite sandstones. **75**, Istituto di Geologia, Università di Parma.
- PERRODON, A. 1985 Dynamics of oil and gas accumulation. *Bulletin des Centres Recherches Exploration-Production, Elf-Aquitane, Pau, France*, pp. 98–105.
- SIMPSON, J. E. 1987 *Gravity Currents in the Environment and the Laboratory*. Ellis Horwood.
- SMITH, P. C. 1973 A similarity solution for slow viscous flow down an inclined plane. *J. Fluid Mech.* **58**, 275–288.
- SPARKS, R. S. J., BONNECAZE, R. T., HUPPERT, H. E., LISTER, J. R., MADER, H., PHILLIPS, J. & HALLWORTH, M. A. 1993 Sediment-laden gravity currents with reversing buoyancy. *Earth Planet. Sci. Lett.* **114**, 243–257.
- TURNER, J. S. 1973 *Buoyancy Effects in Fluids*. Cambridge University Press.
- WESSER, O. E. 1977 Deep-water oil sand reservoirs – ancient case histories and modern concepts. *AAPG Continuing Education Course Notes Series 6*.
- WHITAKER, S. 1984 *Introduction to Fluid Mechanics*. Robert E. Kreiger Publishing Company, Malabar, Florida.